

the Rouse models provides a general description of the dynamical behavior on length scales up to 40 Å and time scales to the 10<sup>-8</sup>-s region. Deviations of the experimental line shape from that predicted by the Rouse model cannot be attributed to local reptation. Thus, an influence of entanglement constraints is not visible on the experimental length and time scales. The experiments in semidilute solutions led to the first direct observation of hydrodynamic screening on a microscopic scale and allowed an evaluation of the hydrodynamic screening length  $\xi_H$ . Its magnitude is close to that of the excluded volume screening length  $\xi_e$  which we have determined recently on the similar system PDMS/C<sub>6</sub>D<sub>6</sub>. This result disagrees with the theoretical prediction  $\xi_H \approx 4\xi_e$ , supposedly valid in the semidilute regime. Perhaps the discrepancy results from using too concentrated systems in our study. More experiments in the semidilute regime are necessary in order to solve this problem and to extract the concentration exponent for  $\xi_H$ . Line-shape arguments as well as the quantitative evaluation

of our data support strongly the model of incomplete screening. The viscosity  $\eta$  which appears in incomplete screening is not yet interpreted on a microscopic level. It exhibits startling similarities to the macroscopic viscosity of an equivalent but nonentangled PDMS solution of smaller molecular weight. In concentrated solution above  $c = 45\%$  enhanced Rouse relaxation prevails. Microscopically determined segmental friction coefficients compare well with those taken from zero shear viscosity measurements. This agreement demonstrates the basic correctness of the molecular foundations of the Rouse model.

*Acknowledgment.* We thank Dr. B. Lehnen for providing the PDMS and Dr. J. B. Hayter for assistance during the experiments. This work was supported in part by the Bundesministerium für Forschung und Technologie and by the Deutsche Forschungsgemeinschaft (Sonderforschungsbereich 41).

Registry No. Neutron, 12586-31-1.

## Electron Spin Resonance Studies on Ordering and Rotational Diffusion in Oriented Phosphatidylcholine Multilayers: Evidence for a New Chain-Ordering Transition

Hisao Tanaka<sup>†</sup> and Jack H. Freed\*

Baker Laboratory of Chemistry, Cornell University, Ithaca, New York 14853 (Received: June 12, 1984)

An alignment technique based on compression has been developed for preparation of planar oriented lipid samples for ESR. The ESR spectra of defect-free samples prepared by this technique could be studied over a wide temperature range, showing gel and liquid-crystalline phases of DPPC and DMPC. The ESR spectra of spin-labeled DPPC's and cholestane clearly indicate a new phase transition occurring at 100–110 °C in the liquid-crystalline phases of DPPC and DMPC hydrated to 3 wt % water with somewhat higher temperatures for higher water content. The extensive spectra that were obtained could be analyzed in detail with a model of anisotropic molecular rotation in a mean orienting potential by using the methods of spectral analysis previously developed by Freed and co-workers. On the basis of the results on molecular ordering and rates of rotational diffusion, the new phase transition is characterized as one in which orientational order is significantly reduced but the rate of molecular motions is not drastically changed. This is compared with a recent theoretical model, which predicts a similar high-temperature transition. The present results also reveal some new aspects regarding hydrocarbon chain motion and disorder in the crystalline phase.

### I. Introduction

In recent years, some new phase transitions have been found for dipalmitoylphosphatidylcholine (DPPC) and dimyristoylphosphatidylcholine (DMPC). These consist of weak transitions occurring below<sup>1</sup> and above<sup>2</sup> the temperature of the main transition,  $T_c$  (gel-liquid crystalline transition), as well as a metastable transition below  $T_c$ ,<sup>3</sup> that are observed with lipid systems containing excess water. Fine structure<sup>4,5</sup> (i.e. successive pretransitional phenomena) occurring in the range of the main transition has also been observed with lipids hydrated to low water content. However, phase diagrams for the higher temperature range ( $\geq 100$  °C) have not been studied as extensively.<sup>6-10</sup> We have found, in this study, a new phase transition occurring at 100–110 °C in the liquid-crystalline phase of DPPC and DMPC hydrated to low content ( $\leq 7\%$ ).

The purpose of this study with spin-labeled DPPC and with cholestane (CSL) is to assign DPPC and DMPC phases (and phase transitions) found from ESR spectra and to characterize them with respect to ordering of the chain and its motion. This is accomplished by determining the ordering and diffusion constants of the nitroxide spin-labels using the ESR line-shape analysis valid over the slow- and fast-motional regime that has been developed in this laboratory.<sup>11-15</sup> The present work was motivated by an effort<sup>16</sup> to study the protein-lipid interaction with the present objective being to obtain precise data on the pure lipids as standard

systems to compare with the complex ESR spectra<sup>16</sup> of samples containing protein (polypeptide).

In order to accomplish the above objectives, we sought a reliable alignment technique for preparation of oriented ESR samples.

- (1) (a) Chen, S. C.; Sturtevant, J. M.; Gaffney, B. J. *Proc. Natl. Acad. Sci. U.S.A.* **1980**, *77*, 5060. (b) Buocco, M. J.; Shipley, G. G. *Biochim. Biophys. Acta* **1982**, *691*, 309.
- (2) (a) Furuya, K.; Mitsui, T. *J. Phys. Soc. Jpn.* **1979**, *46*, 611. (b) Albrecht, O.; Gruler, H.; Sachmann, E. *J. Phys. (Orsay, Fr.)* **1978**, *39*, 301.
- (3) Curataro, W.; Boli, A.; Gupta, C. M. *Biochim. Biophys. Acta* **1982**, *690*, 89.
- (4) Doniaech, S. *J. Chem. Phys.* **1979**, *70*, 4587.
- (5) Kodama, M.; Kuwabara, M.; Seki, S. *Biochim. Biophys. Acta* **1982**, *689*, 567.
- (6) Chapman, D.; Williams, R. M.; Lodbrooke, B. D. *Chem. Phys. Lipids* **1967**, *1*, 445.
- (7) Luzzati, V.; Tardieu, A. *Annu. Rev. Phys. Chem.* **1974**, *25*, 791.
- (8) Janiak, M. J.; Small, D. M.; Shipley, G. G. *Biochemistry* **1976**, *15*, 4575.
- (9) Powers, L.; Pershan, P. S. *Biophys. J.* **1977**, *20*, 137.
- (10) Lentz, B. R.; Freire, E.; Biltonen, R. L. *Biochemistry* **1978**, *17*, 4475.
- (11) (a) Freed, J. H.; Bruno, G. V.; Polnaszek, C. F. *J. Phys. Chem.* **1971**, *75*, 3385. (b) Polnaszek, C. F.; Bruno, G. V.; Freed, J. H. *J. Chem. Phys.* **1973**, *58*, 3185.
- (12) (a) Hwang, J. S.; Mason, R. P.; Hwang, L. P.; Freed, J. H. *J. Phys. Chem.* **1975**, *79*, 489. (b) Polnaszek, C. F.; Freed, J. H. *Ibid.* **1975**, *79*, 2283.
- (13) Moro, G.; Freed, J. H. *J. Phys. Chem.* **1980**, *84*, 2837.
- (14) Moro, G.; Freed, J. H. *J. Chem. Phys.* **1981**, *74*, 3757.
- (15) (a) Meirovitch, E.; Igner, D.; Igner, E.; Moro, G.; Freed, J. H.; *J. Chem. Phys.* **1982**, *77*, 3915. (b) Campbell, R. F.; Meirovitch, E.; Freed, J. H. *J. Phys. Chem.* **1979**, *83*, 525. (c) Meirovitch, E.; Nayeem, A.; Freed, J. H. *Ibid.* **1984**, *88*, 3454.
- (16) Tanaka, H.; Freed, J. H. *J. Phys. Chem.*, in press.

<sup>†</sup>Permanent address: Josai University, Saitama, Japan.

One limitation of the evaporation technique used in previous ESR studies<sup>17-19</sup> is that the macroscopic orientation of the samples prepared as films becomes<sup>19</sup> unstable at higher temperatures. We developed a compression technique on the basis of Asher's alignment method.<sup>20,21</sup> The technique consists of repeating compressions on lipids just above the main transition temperature. The quality of sample orientation was determined by use of polarizing microscopy.<sup>22</sup> We have confirmed that the morphology (as well as the transmitted photointensity) of an oriented sample detected under crossed polarizers closely correlates with the degree of order manifested in the ESR spectra. The procedure of sample preparation and quality control is described in the Experimental Section.

The use of defect-free oriented samples enabled us to clearly observe lipid-phase transitions through the appearance of composite spectra in the transition (two-phase) region. In general, the well-oriented ESR spectra were analyzed with significantly less ambiguity than is possible for those from unoriented systems. From ESR observations on DPPC and DMPC hydrated to 3% water, three phase transitions were found in the temperature range  $\leq 180$  °C: two were assigned to the main transition and to the isotropic transition by reference to the transition temperatures in the literature.<sup>9,18</sup> The remaining one, at 100–110 °C, which was observed most distinctly in the present experiments using oriented lipid samples and hydrocarbon chain (or phosphatidylcholine) spin-labels was characterized as a "chain-orientational" transition from the data analyzed. By this we mean a transition in which the mean ordering of the lipid chains is significantly reduced but with less dramatic effects on the chain dynamics. In a recent theory, Kimura and Nakano<sup>23</sup> have predicted the appearance of what may be a similar orientational transition in the liquid-crystalline phase of DPPC, DMPC, and other lipids. Thus, we believe our observations provide direct evidence for the presence of this orientational transition, as discussed in this paper.

Another aspect of this work focuses on a current topic in magnetic resonance studies on lipid dispersions<sup>24-27</sup> regarding the presence and type of hydrocarbon chain motion and/or disorder in the gel phase, for which the model of a rigid and extended conformation (e.g. all-trans) was established by previous X-ray studies.<sup>6,7,28</sup> In the present work, more detailed aspects of such matters were revealed by our systematic study of ordering, anisotropic diffusion, and their temperature dependence using the different spin probes.

Our experimental methods are described in section II, while our results and spectral analyses are given in section III. These results are discussed in section IV, with a summary and concluding remarks in section V.

## II. Experimental Section

**Materials.** The phosphatidylcholines DPPC and DMPC were purchased from Sigma and checked for purity by thin-layer chromatography according to standard methods.<sup>18</sup> The nitroxide CSL(3-doxy derivative of cholestan-3-one) was obtained from

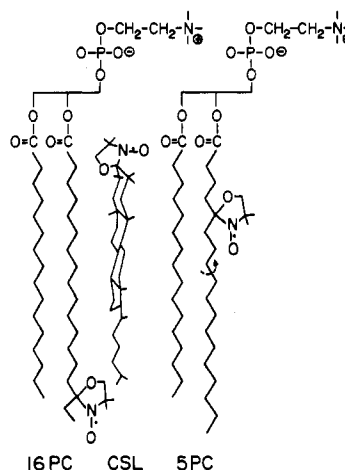


**Figure 1.** Schematic structures of CSL, 5PC, and 16PC. The relation between the molecular axes systems of the ordering axes ( $x', y', z'$ ) and magnetic tensor axes ( $x'', y'', z''$ ) is found by spectral simulation to be  $z' = z''$  for 16PC and 5PC and  $z' = y''$  for CSL.

Synvar, and the DPPC derivative nitroxides<sup>29,30</sup> 5PC and 16PC (DPPC's bonded at 5th and 16th carbon of the hydrocarbon chain by the nitroxide moiety) were a gift from G. W. Feigenson, Department of Biochemistry, Cornell University. These nitroxides are shown in Figure 1. Hexadecyltrimethylammonium bromide (HTAB), purchased from Aldrich and recrystallized from toluene, was used<sup>18</sup> to coat the glass plates used for a sample sandwich. The glass plates ( $0.8 \times 2.2$  cm<sup>2</sup> in area and 130  $\mu$ m in thickness) were cleaned first with chloroform, then hot concentrated sulfuric acid, and then deionized water and were treated with HTAB just before use to promote homeotropic alignment.

Mixtures of lipid with nitroxide were prepared by a freeze-dry method<sup>18</sup> in the following procedure. Typically 25 mg of lipid was put in a 2-mL glass flask with a ground joint. A given volume of benzene-methanol (95:5 v/v) solution of nitroxide was added to the flask to form 0.5 mol % nitroxide mixture with lipid. After complete dissolution of the solutes, the flask was linked to a vacuum line, and the solution was quickly frozen with liquid N<sub>2</sub>. The frozen solution in a dry ice-2-propanol cold bath was evacuated for 2 days at  $10^{-3}$  torr, followed by further evacuation for 2 days at room temperature to ensure solvent removal. The dry solids were crushed to a fine powder and were hydrated to a water content below 20 wt %. A homogeneous distribution of water in the lipid layer was promoted by gas-solid absorption. It consists of separately placing a proper amount of deionized water and the powdered mixture inside the flask sealed under Ar atmosphere. After being kept for a week at room temperature in the dark, the hydrated mixture was aligned as described below.

**Alignment Procedure with the Compression Technique.** Sample holders for compression were made of a Mylar sheet stuck on the surface of a microscope glass slide and designed to form a cavity at the center. A surfactant-treated glass plate was placed in the cavity of the holder fixed onto the heating stage. Subsequently, 3 mg of hydrated lipid mixture was spread on the glass, away from the edge, and was covered by the second glass plate and then by the top holder. The assembly was heated to above the main transition temperature ( $T_c$ ) while pressed from the top. The optimal temperature for compression, corresponding to the softening temperature of the hydrated lipid, depends on water content (65–80 °C on going from 15 to 2 wt % water in DPPC). At the appropriate temperature, the sandwiched sample was compressed with pressure applied from above but translated in strokes of several seconds duration across the surface. After the process was repeated for several minutes, the lipid layer became spread to a thin layer (5–20  $\mu$ m). After the above procedure, the sample assembly, with pressure applied from the top, was cooled to room

(17) Jost, P.; Libertini, L. T.; Herbert, V. C.; Griffith, O. H. *J. Mol. Biol.* **1971**, *59*, 77.

(18) Marsh, D. *Can. J. Biochem.* **1974**, *52*, 631.

(19) (a) Smith, I. C. P.; Butler, K. W. In "Spin Labeling—Theory and Applications"; Berliner, L. J., Ed.; Academic Press: New York, 1976. (b) Schreier, S.; Polnaszek, C. F.; Smith, I. C. P. *Biochim. Biophys. Acta* **1978**, *515*, 395. (c) Butler, K. W.; Smith, I. C. P. *Can. J. Biochem.* **1978**, *56*, 117.

(20) Asher, S. A.; Pershan, P. S. *Biophys. J.* **1979**, *27*, 393.

(21) There may be some similarity of our method to the aligning technique of Hemminga and Berendsen (*J. Magn. Reson.* **1972**, *8*, 133), who however give few details. While they appear to use shearing, the well-documented Asher-Pershan method,<sup>20</sup> which we have adapted, crucially depends upon annealing and compression.

(22) (a) Powers, L.; Clark, N. A.; *Proc. Natl. Acad. Sci. U.S.A.* **1975**, *72*, 840. (b) Powers, L. Thesis, Harvard University, 1977.

(23) (a) Kimura, H.; Nakano, H. *J. Phys. Soc. Jpn.* **1977**, *43*, 1447; **1979**, *46*, 1695. (b) Kimura, H.; Nakano, H. *Mol. Cryst. Liq. Cryst.* **1981**, *68*, 289.

(24) Davis, J. H. *Biophys. J.* **1979**, *27*, 339.

(25) Marsh, D. *Biochemistry* **1980**, *19*, 1632.

(26) MacKay, A. L. *Biophys. J.* **1981**, *35*, 301.

(27) Trahms, L.; Klabe, W. D.; Boroske, E. *Biophys. J.* **1983**, *42*, 285.

(28) Träuble, H.; Haynes, P. *Chem. Phys. Lipids* **1971**, *7*, 324.

(29) Hubbell, W. L.; McConnell, H. M. *J. Am. Chem. Soc.* **1971**, *93*, 314.

(30) Boss, W. F.; Kolley, C. J.; Landsberger, F. R. *Anal. Biochem.* **1975**, *64*, 289.

temperature at a rate of 1–2 °C/min. An excess of the starting lipid material leaking out of the sample sandwich was removed, and the sandwich was sealed on its edges with epoxy or some other adhesive.

Skillful use of this technique can provide substantially defect-free ( $\leq 3\%$  of defect area) oriented lipid samples at comparatively low temperatures ( $\leq 80$  °C) and in a short period of time ( $\leq 1$  h). Furthermore, the planar orientation of the lipid multilayer between the glass plates remains stable as the ESR spectra are recorded, without the appearance of any defects, over the full temperature range including the gel and liquid-crystalline phases. The defect-free samples used for ESR measurements were prepared as multilayers with a typical thickness of 10  $\mu\text{m}$  ( $\sim 2000$  bilayers) containing a monodomain with at worst a few small air bubbles.

The water content in a sample was calibrated with  $^1\text{H}$  NMR measurements of a nitroxide-free reference sample prepared in the same manner as the ESR samples. The oriented sample was crushed in a small vial and extracted with 400  $\mu\text{L}$  of deuterated benzene–chloroform (2:1 v/v) mixture. The  $^1\text{H}$  NMR spectrum of extract was recorded on a Varian 90-MHz CFT-20 pulse spectrometer. The water content was determined from the relative intensity of the water signal ( $\delta$ : 2.3–2.8 ppm, referred to  $\text{Me}_2\text{Si}$ ) vs. the trimethylammonium group of the lipid (cf. Figure 1) ( $\delta = 3.3$  ppm). The main transition temperature ( $T_c$ ) was determined from the ESR spectrum of the corresponding nitroxide sample prepared at the same time and in the same manner. Thus, the water content of subsequent ESR samples was determined according to the relation  $T_c/^\circ\text{C} = -1.5 \times [\text{water}] + 77$  (for samples  $\leq 15$  wt % of water). This relation was established from the sets of NMR and ESR samples of different water content. Accuracy is expected to be  $\pm 1$  to  $\pm 2$  wt %.

**Characterization of Oriented ESR Samples.** An incomplete procedure for sample alignment leaves unoriented areas (defects) in the sample. Defects are also produced through dilations of the sample sandwich, rapid change of temperature, etc. In the course of establishing our alignment technique and the conditions for ESR measurements, we observed several types of defects using a polarizing microscope. These are, according to the morphological nomenclature used in the previous literature,<sup>17</sup> amorphous type (i.e. starting with unoriented materials), polygonal-array type, oily streak type, and strandlike type. These defects were observed under crossed polarizers to study the conditions of their appearance and evolution and also to estimate their area relative to the remaining oriented region by utilizing measurement of the transmitted photointensity.<sup>31</sup> In general, defects in thin samples ( $< 30$   $\mu\text{m}$ ) were observed as white (bright) areas. The ESR spectra of samples containing defects are composed of two components of which the one assigned to defects exhibits no detectable angular dependence of the hyperfine splittings on rotation of the plate sample. Such spectral features were observed only under the conditions where the respective type of defect could be observed under crossed polarizers. For example, the amorphous type of defect is stable below and above  $T_c$ , while the polygonal type only appears above  $T_c$ . Although clear observation of the defect signal depended on such factors as the particular nitroxide used, the temperature, water content, etc., the signal intensity observed with CSL samples was found to be proportional to the defect area estimated optically. From these facts as well as some others, it was judged that the quality of the ESR sample alignment is decisively determined by the presence of defects detected optically. The samples which contained substantially no defects ( $\leq 3\%$ ) produced a simple triplet pattern<sup>32</sup> of nitroxide over the temperature range studied except in the phase transition region, as discussed in the next section. Because of the importance of recognizing and eliminating defects for any careful ESR studies

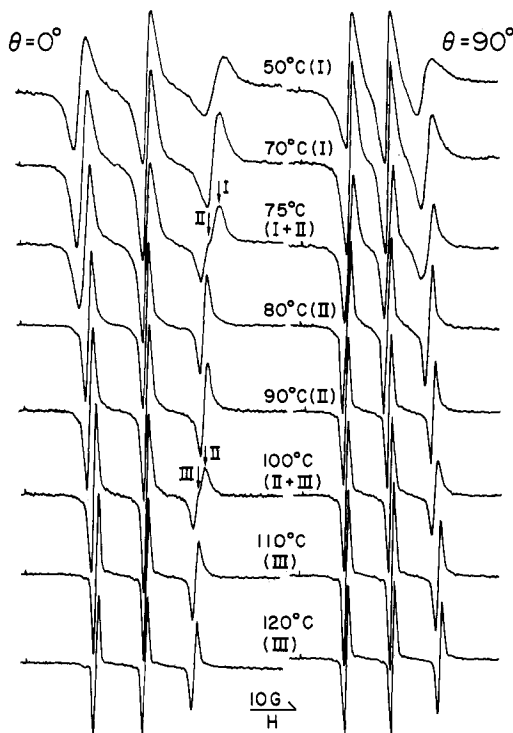


**Figure 2.** ESR spectra of 16PC in oriented DPPC multilayers with 3 wt % hydration. Phase transitions are observed at 75 and 100 °C. Phase I, below 75 °C, is the biaxial gel phase. Phases II and III are liquid-crystalline  $L_\alpha$  phases.

on oriented samples, we provide further discussion on these matters in the Appendix.

**Polarizing Microscopy and ESR Measurements.** Oriented lipid samples were observed by a polarizing microscope, a Nikon OPTIPHOTO-POL, before and after ESR measurement. A Mettler FP5-FP-52 temperature control accessory attached to the microscope was used for observation of defects at higher temperatures. Transmitted photointensity under crossed polarizers was measured with a Mettler 18100 photoresistor recording unit attached to the microscope.

For ESR measurements, a sample attached to a goniometer was placed in a Varian TE 011-mode cavity. The ESR spectra were recorded on a Varian E-12 spectrometer at X band with 100-kHz field modulation. The temperature of the sample was controlled with a Varian 257 accessory and was read from an OMEGA 410A-TC digital thermometer with a fine copper-constantan thermocouple, one terminal of which was placed at the center of sample plate. The estimated uncertainty in temperature was  $\pm 1$  °C. The temperature of sample was only changed slowly to avoid producing defects. The ESR spectra were usually taken every 5 °C, at  $\theta = 0$  and  $90^\circ$  (the normal to the sample plate parallel and perpendicular to the external magnetic field, respectively) and at intermediate values of  $\theta$  at some temperatures in each phase. The reproducibility of the ESR spectra was checked by comparing the spectra taken at the same temperature in both heating and cooling cycles. The main transition temperature ( $T_c$ ) observed in both processes was used to estimate any loss of hydrated water at higher temperatures. The microwave power and the modulation amplitude employed were low enough so as not to affect the ESR line shapes. We confirmed that there was no broadening for the nitroxide concentration (0.5 mol %) used from intermolecular spin interactions (e.g., Heisenberg spin exchange interaction).

### III. Experimental Results and Spectral Analysis

The temperature dependence of the experimental spectra of the oriented lipid samples is shown for 16PC in DPPC and CSL in DMPC hydrated to 3%, in Figures 2 and 3, respectively. In the former spectra, phase transitions are observed at 75 and 100 °C, where two-phase spectra due to components from the upper and

(31) Petrov, A. G.; Gawzish, K.; Brezinsinski, G.; Klose, G.; Möps, A. *Biochim. Biophys. Acta* **1984**, *690*, 1.

(32) One pattern (a simple triplet) should not necessarily be expected for the general case. For example, in defect-free oriented lipid samples containing gramicidin (polypeptide), the ESR spectral feature was found to be of a two-component type, as shown in ref 16.

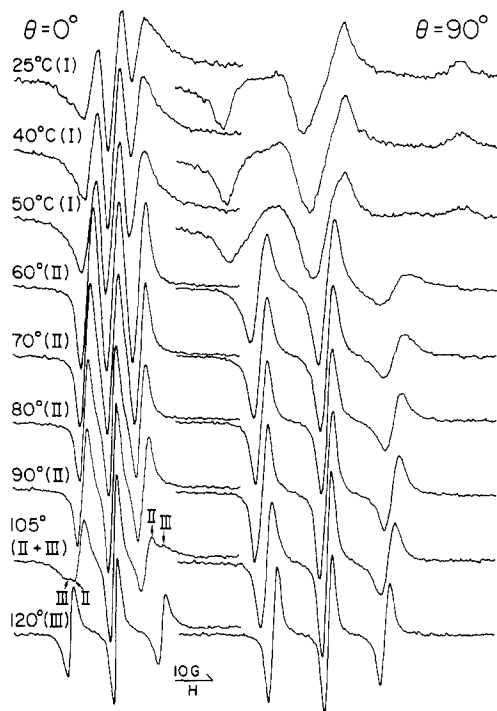


**Figure 3.** ESR spectra of CSL in oriented DMPC multilayer hydrated to 3 wt %. Phase transitions occur between 50 and 60 °C and between 95 and 115 °C.

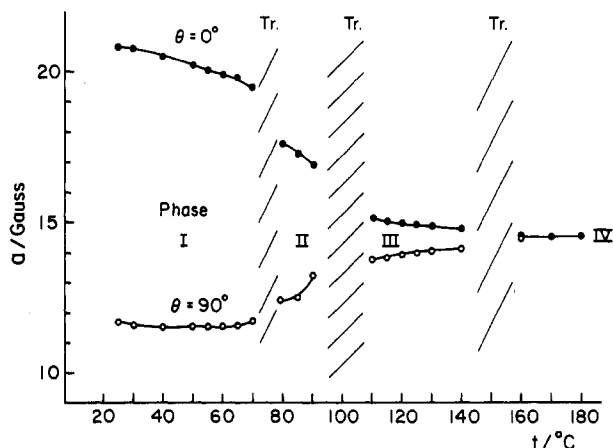


**Figure 4.** Temperature dependence of the apparent line splittings of 16PC in oriented DPPC multilayer hydrated to 3 wt %: I, biaxial gel phase; II and III, liquid-crystalline phases; IV, isotropic phase. The splittings were measured between the centers of  $M_1 = 0$  and 1 lines.

lower temperature ordered phase(s) may be seen. The apparent hyperfine splittings are plotted as a function of temperature up to 180 °C in Figure 4. From this figure, we can find the third transition in the range of 140–160 °C, leading to angular ( $\theta$ )-independent ESR spectra. In DMPC hydrated to 3% (Figure 3), the first and second transitions were observed between 50 and 60 °C and between 95 and 115 °C, respectively. In the respective ordered phases I, II, and III (with increasing temperature), the observed line splitting was a maximum for CSL and a minimum for 5PC and 16PC at  $\theta = 90^\circ$  (i.e. normal to the bilayer plane perpendicular to the external magnetic field) with an experimental error ( $\pm 2^\circ$ ) in sample setting. Figure 5 shows plots of splitting with  $\theta$  for CSL and 16PC in phase I. The ESR spectra of 5PC in phase II at different  $\theta$ 's are shown in Figure 6.

With an increase of the water content in DPPC, the temperature of the first transition decreased monotonically to 50 °C; i.e.  $T_c$  is  $75 \pm 3$  °C at 3% water, 66 °C at 7%, 57 °C at 12%, and 52 °C at 15%. The temperature of the second transition tended to increase from 100 °C at 3% water to 110 °C at 7%. The second transition temperature in samples hydrated at higher water content

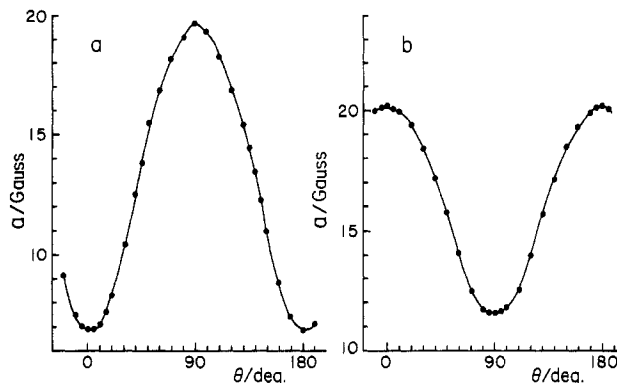


**Figure 5.** Angular ( $\theta$ ) dependence of the line splittings of CSL (a) and 16PC (b) in oriented DPPC multilayers of 3 wt % water content at 60 °C (phase I). The splittings were measured between the centers of  $M_1 = 0$  and 1. In both cases, the minimum and maximum were observed at  $\theta = 0$  and  $90^\circ$  within an error of  $2^\circ$ .

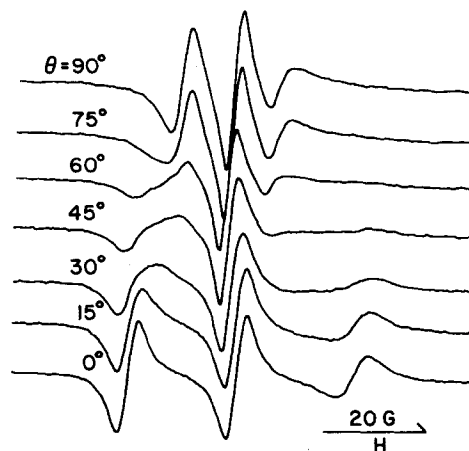


**Figure 6.** Angular ( $\theta$ ) dependence of the ESR spectra of 5PC in oriented DPPC hydrated to 10%, recorded at 70 °C (phase II). The minimum and maximum in the splitting are observed at  $\theta = 0$  and  $90^\circ$ , respectively.

could not be measured because of the greater loss of water from the sample sandwich at the high temperatures. Where no loss of the water occurred (i.e. at lower hydration), reproducibility of the spectra and transition temperatures was observed in the heating and cooling cycles. Judging from spectral characteristics on phase transitions, the two-phase range (transition range) was wider in the second transition ( $\sim 20^\circ$ , e.g. 90–110 °C for 3 wt %  $H_2O$ -DPPC) than in the first one ( $\sim 10^\circ$ ).<sup>33</sup> From comparison of the above results on transition temperatures with the phase diagrams<sup>6,9</sup> of DPPC and DMPC hydrated at low water contents, the first transition can be assigned to the main transition (gel-liquid crystalline transition; we shall follow Powers and Pershan<sup>9</sup> who classified the low-temperature phase as a biaxial gel phase). The isotropic transition was previously observed with a conoscopic birefringence method<sup>20,22</sup> as a transition from an optically uniaxial phase to an isotropic phase (135–160 °C in DPPC hydrated to 2%–8%). Thus, the third transition in this work is regarded as identical with the optically isotropic transition. In section IV, we will discuss the character of the second transition found in this study.

The ESR spectra of the oriented samples were analyzed by use of the method of line-shape analysis described in detail elsewhere.<sup>13,14</sup> This analysis involves the following coordinate systems: the first ( $x, y, z$ ) is the laboratory frame with the  $z$  axis along the external magnetic field. A second ( $x'', y'', z''$ ) is the principal axis system of the magnetic tensor of the molecule **A** (with an arbitrary tilt of **g** relative to **A** allowed but not needed in this work). A third ( $x''', y''', z'''$ ) is the ordering axis (which is taken as the same as the rotational diffusion axis) system of the molecule. The last

(33) Gottlieb, M. H.; Evans, E. D. *Biophys. J.* 1974, 14, 335.

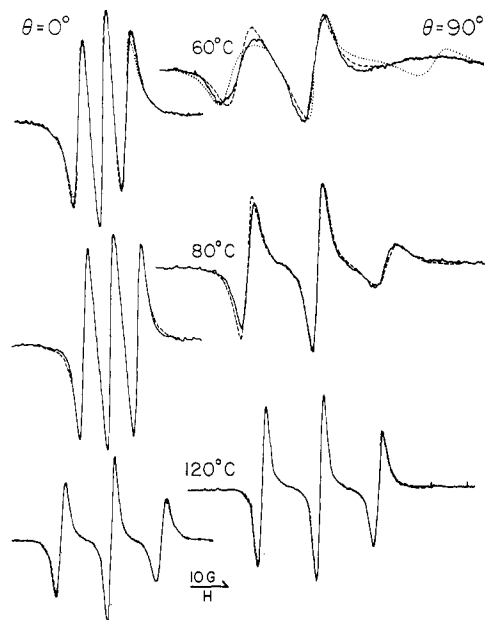


**Figure 7.** Comparison of the experimental (—) and best-fit calculated (---) spectra of CSL in oriented DPPC multilayer hydrated to 3 wt %, shown at 60 °C (phase I), 80 °C (phase II), and 120 °C (phase III). The constants used for the simulation are listed in Table I. The calculated spectra (---) at 60 °C exemplify an effect of  $N$  ( $N = 100$  but the other constants are the same as those at 60 °C in Table I).

one ( $x'', y'', z''$ ) denotes the director frame characterizing the long-range order of the molecules in the ordered phases. One can designate the angle ( $\theta$ ) between the director ( $z''$  axis) and the magnetic field ( $z$  axis). The transformation of the magnetic tensor axes to the ordering axis system leads us to discriminate a nitroxide as a  $x'''$ -,  $y'''$ -, or  $z'''$ -ordering nitroxide (e.g.,  $z' \equiv z'''$  for 16PC and 5PC and  $z' = y'''$  for CSL), as already observed by rotation of the plate sample. The tilt between the ( $x', y', z'$ ) and ( $x'', y'', z''$ ) molecular axis systems is represented by the Euler angles  $\alpha$ ,  $\beta$ , and  $\gamma$ . The potential function determining molecular ordering is expanded in a series of Wigner rotation matrix elements

$$V/kT = \sum_{L,M,K} C_{MK}^L D_{MK}^L(\Omega) = \lambda D_{00}^L + \rho(D_{02}^L + D_{0-2}^L) + \epsilon D_{00}^L + \dots$$

where  $C_{MK}^L$ ,  $\lambda$ ,  $\rho$ , and  $\epsilon$  are dimensionless coefficients of the respective terms and  $\Omega$  represents the Euler angles between the ( $x', y', z'$ ) coordinates and the ( $x'', y'', z''$ ) coordinates.

The principal values of  $\mathbf{A}$  were determined as follows.  $A_{z''}$  was measured from the outermost splittings in the ESR spectrum of the unoriented lipid sample in a cylindrical tube at liquid  $N_2$  temperature ( $33.5 \pm 0.5$  G for CSL and  $33.0 \pm 0.5$  G for 16PC and 5PC). The  $A_{x''}$  ( $= A_{y''}$ ) was derived from the relation  $a_N = (A_{x''} + A_{y''} + A_{z''})/3$  taken with  $A_{z''}$  and the isotropic coupling  $a_N$  (14.6 G for CSL and 14.4 G for 16PC and 5PC) found in the isotropic phase. The principal values of  $\mathbf{g}$  were adopted from those<sup>34</sup> for CSL doped in a single crystal of cholesteryl chloride. The above values of  $\mathbf{A}$  and  $\mathbf{g}$  were allowed a small variation in our simulations to refine them so as to optimize the fits to both the  $\theta = 0$  and  $90^\circ$  oriented spectra, recorded over a wide temperature range. The values of  $\mathbf{A}$  we finally obtained are  $A_{z''} = 33.8$  G and  $A_{x''}$  ( $= A_{y''}$ ) = 5.0 G for CSL and  $A_{z''} = 33.0$  G and  $A_{x''}$  ( $= A_{y''}$ ) = 4.9 G for 16PC and 5PC. Those of  $\mathbf{g}$  are  $g_{x''} = 2.0089$ ,  $g_{y''} = 2.0058$ , and  $g_{z''} = 2.0021$  for all the nitroxides.

The spectral simulation process was started using a minimal set of parameters: the primary potential term  $\lambda$  corresponding to cylindrically symmetric ordering as well as the parallel and perpendicular rotational diffusion coefficients  $R_{\parallel}$  and  $R_{\perp}$  with a fixed anisotropy ratio  $N (= R_{\parallel}/R_{\perp})$ . At the next step,  $N$  was allowed to be different in each phase. This latter procedure

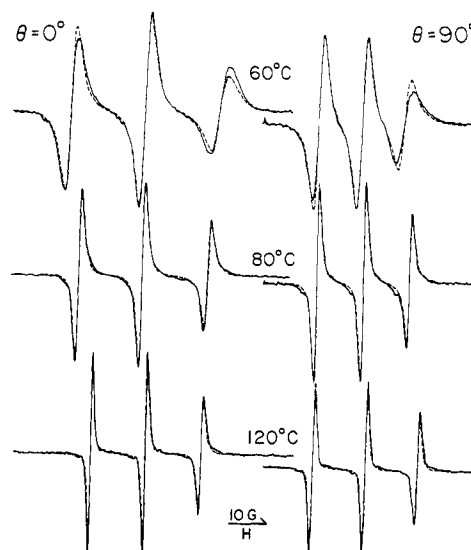


**Figure 8.** Comparison of the experimental (—) and best-fit calculated (---) spectra of 16PC in oriented DPPC hydrated to 3 wt %, shown at 60 °C (phase I), 80 °C (phase II), and 120 °C (phase III). The constants used for the simulation are listed in Table II.

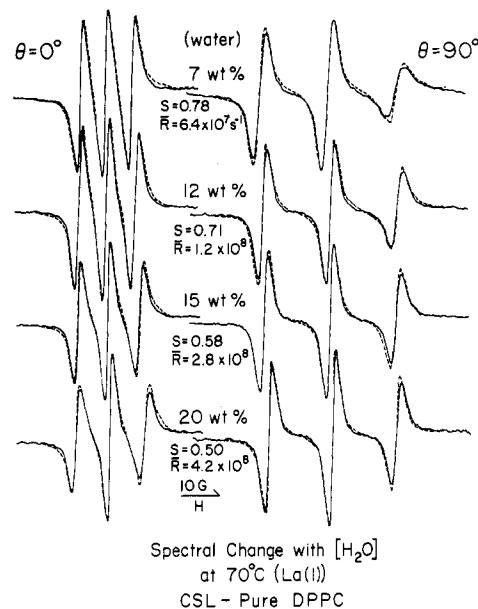


**Figure 9.** Water content dependence of the ESR spectra of CSL in oriented DPPC, recorded at 70 °C (phase II): (—), experimental spectrum; (---), best-fit calculated spectrum. The other constants are as follows:  $\langle D_{02}^L + D_{0-2}^L \rangle = -0.01$  at 7 and 12 wt % water and 0 at 15 and 20 wt %;  $R_{\perp} = 9.0 \times 10^6$  at 7%,  $1.7 \times 10^7$  at 12%,  $4.0 \times 10^7$  at 15%, and  $6.0 \times 10^7$  at 20%;  $N = 50$  and  $T_2^{*-1} = 1.2$  G at all the water contents.

noticeably improved the fit between calculated and experimental spectra and is illustrated in Figure 7. Finally, a second term in the potential,  $\rho$ , which yields deviations from cylindrically symmetric ordering, was introduced into the simulations (mainly for fine adjustment of the relative peak heights of the  $M_1 = \pm 1$  lines). The optimal fits for both the  $\theta = 0$  and  $90^\circ$  spectra were obtained with the four parameters  $\lambda$ ,  $\rho$ ,  $R_{\perp}$ , and  $N$ , as illustrated with some spectra of CSL and 16PC in Figures 7–9. (In past studies on thermotropics<sup>15a</sup> we have found that spectra from these two orientations are usually sufficient to obtain a definitive set of parameters.) The ordering and diffusion constants determined for CSL, 16PC, and 5PC in DPPC hydrated to 3% are listed in Tables I, II, and III, respectively, together with the estimated errors in the respective constants. Additional results for 7% hydration may be found in Tables IB and IIB. In the tables,  $T_2^{*-1}$  denotes the residual (largely inhomogeneous) line width. The

TABLE I: Parameters for Molecular Ordering and Anisotropic Rotation of CSL in DPPC<sup>a</sup>

$t, ^\circ\text{C}$	phase <sup>b</sup>	$\langle D_{00}^2 \rangle^d$	$\langle D_{02}^2 + D_{0-2}^2 \rangle^d$	$R_{\perp}, ^\circ\text{s}^{-1}$	$R_{\parallel}, ^\circ\text{s}^{-1}$	$N$	$E_a, \text{kcal/mol}$	$T_2^{*-1}, \text{G}$
(A) Hydrated to 3 wt %								
40	I	0.90	-0.01	$2.9 \times 10^5$	$4.4 \times 10^7$	150	7.7	1.5
50		0.90	-0.01	$4.0 \times 10^5$	$6.0 \times 10^7$			
60		0.90	-0.01	$6.2 \times 10^5$	$9.3 \times 10^7$			
70		0.90	-0.01	$8.3 \times 10^5$	$1.2 \times 10^8$			
80	II	0.76	-0.03	$6.8 \times 10^6$	$3.4 \times 10^8$	50	(8.7)	1.2
85		0.73	-0.03	$8.0 \times 10^6$	$4.0 \times 10^8$			
90		0.67	-0.03	$9.6 \times 10^6$	$4.8 \times 10^8$			
110	III	0.28	0.08	$1.1 \times 10^8$	$1.7 \times 10^9$	16	9.2	1.0
120		0.21	0.06	$1.5 \times 10^8$	$2.4 \times 10^9$			
130		0.14	0.03	$2.0 \times 10^8$	$3.2 \times 10^9$			
140		0.13	0.03	$2.5 \times 10^8$	$4.0 \times 10^9$			
160	IV	0	0	$5.8 \times 10^8$	$2.9 \times 10^9$	5	5.0	1.0
170		0	0	$6.7 \times 10^8$	$3.4 \times 10^9$			
180		0	0	$7.5 \times 10^8$	$3.8 \times 10^9$			
(B) Hydrated to 7 wt %								
40	I	0.88	-0.005	$3.0 \times 10^5$	$4.5 \times 10^7$	150	(8.7)	1.5
50		0.88	-0.005	$5.0 \times 10^5$	$7.5 \times 10^7$			
60		0.88	-0.005	$7.0 \times 10^5$	$10.5 \times 10^7$			
70	II	0.78	-0.007	$9.0 \times 10^6$	$4.5 \times 10^8$	50	(7.0)	1.2
80		0.74	-0.009	$1.2 \times 10^7$	$6.0 \times 10^8$			
90		0.65	-0.015	$1.6 \times 10^7$	$8.0 \times 10^8$			

<sup>a</sup> Estimated errors:  $\pm 2\%$  in  $\langle D_{00}^2 \rangle$ ,  $\pm 30\%$  in  $\langle D_{02}^2 + D_{0-2}^2 \rangle$ ,  $\pm 10\%$  in  $R_{\perp}$ ,  $\pm 20\%$  in  $N$ ,  $\pm 20\%$  in  $E_a$ , and  $\pm 0.1 \text{ G}$  in  $T_2^{*-1}$ . Note  $R_{\parallel} = NR_{\perp}$ . <sup>b</sup> I, biaxial gel phase; II and III, liquid-crystalline phases; IV, isotropic phase. <sup>c</sup> Correlation times:  $\tau_{\perp} = 1/6R_{\perp}$ ,  $\tau_{\parallel} = 1/6R_{\parallel}$ , and  $\bar{\tau} = 1/6\bar{R} = 1/6(R_{\parallel}R_{\perp})^{1/2}$ . <sup>d</sup> The relationship between  $\langle D_{00}^2 \rangle$  and  $\lambda$  and  $\rho$  is given by the following expression:

$$\langle D_{00}^2 \rangle = \int \phi' f_{\theta'} P(\theta', \phi')^{1/2} (3 \cos^2 \theta' - 1) \sin \theta' d\theta' d\phi'$$

and  $\langle D_{02}^2 + D_{0-2}^2 \rangle = \int \phi' f_{\theta'} P(\theta', \phi') (6^{1/2}/2) \sin^2 \theta' \cos 2\phi' \sin \theta' d\theta' d\phi'$ , where  $\theta'$  denotes the angle between the principal axis  $z'$  of the ordering tensor and the principal axis  $z''$  of the director frame.  $P(\theta', \phi')$  is the distribution of  $z'$  relative to  $z''$  given by  $P(\theta', \phi') \propto \exp[-\lambda/2(3 \cos^2 \theta' - 1) + (6^{1/2}/2)\rho \sin^2 \theta' \cos 2\phi']$ .

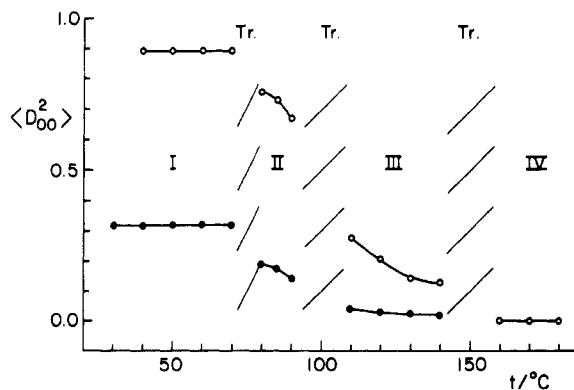


Figure 10. Plots of the ordering  $\langle D_{00}^2 \rangle$  ( $\equiv S$ ) vs. temperature for CSL (●) in oriented DPPC hydrated to 3 wt % and 16PC (○) in oriented DPPC hydrated to 3%: I, biaxial gel phase; II and III, liquid-crystalline phases; IV, isotropic phase.

values of  $T_2^{*-1}$  were found to be constant to within 0.1 G with respect to varying the angle  $\theta$  from 0 to 90° in each phase. The ordering parameter  $\langle D_{00}^2 \rangle \equiv S$  and  $\bar{R}$  values of CSL and 16PC are plotted vs. temperature in Figures 10–12. (The ordering parameters are directly calculated from the potential terms  $\lambda$  and  $\rho$  as shown in the caption to Table I.) As seen in Table III, the spectra of 5PC were analyzed with only the parameters  $\lambda$ ,  $R_{\perp}$ , and  $N$ . It was difficult to evaluate the subtle effect of  $\rho$  in 5PC because the spectra exhibited some contribution due to a small amount of director distribution possibly due to a collective chain-tilting phenomenon.<sup>35</sup>

It should be noted that, especially for the 5PC and 16PC spin-labels, the actual motions can be quite complex, including overall motion of the labeled lipid with many internal modes of motion of the flexible hydrocarbon chain to which the nitroxide moiety is attached. The spectral sensitivity to such complex motions is, however, limited, and we find, in general, that simpler

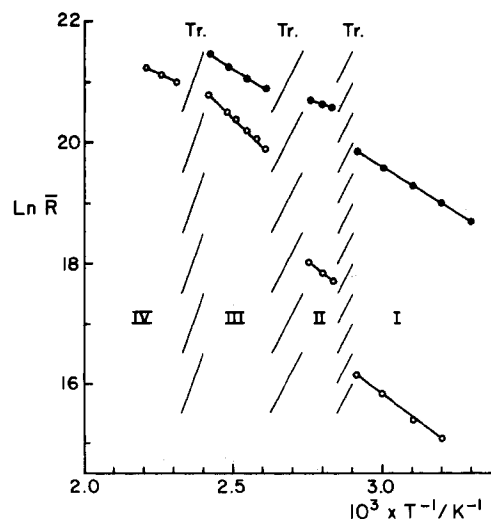


Figure 11. Arrhenius plots of the mean diffusion constant  $\bar{R}$  ( $\equiv (R_{\perp}R_{\parallel})^{1/2}$ ) for (●) CSL in oriented DPPC hydrated to 3 wt % and (○) 16PC in oriented DPPC hydrated to 3%: I, biaxial gel phase; II and III, liquid-crystalline phase; IV, isotropic phase.

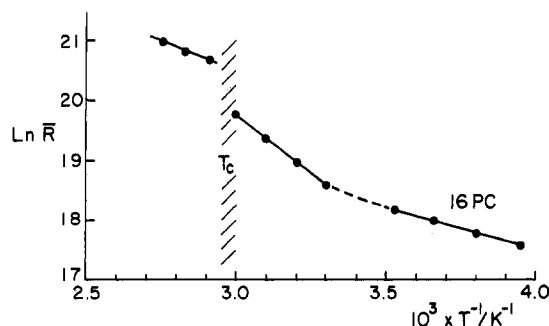


Figure 12. Arrhenius plots of the mean diffusion constant  $\bar{R}$  of 16PC in oriented DPPC hydrated to 7% based on values in Table IIIB.

(35) Stamatoff, J. B.; Graddick, W. F.; Powers, L.; Moncton, D. E. *Bio-phys. J.* **1979**, *25*, 2536.

TABLE II: Parameters for Molecular Ordering and Anisotropic Rotation for 16PC in DPPC<sup>a, b</sup>

$t, ^\circ\text{C}$	phase	$\langle D_{00}^2 \rangle$	$\langle D_{02}^2 + D_{0-2}^2 \rangle$	$R_{\perp}, \text{s}^{-1}$	$R_{\parallel}, \text{s}^{-1}$	$N$	$E_a, \text{kcal/mol}$	$T_2^{*-1}, \text{G}$
(A) Hydrated to 3 wt %								
30	I	0.32	-0.17	$9.3 \times 10^7$	$1.9 \times 10^8$	2.0	6.1	1.4
40		0.32	-0.17	$1.8 \times 10^8$	$3.6 \times 10^8$			
50		0.32	-0.17	$2.4 \times 10^8$	$4.8 \times 10^8$			
60		0.32	-0.17	$3.3 \times 10^8$	$6.6 \times 10^8$			
70		0.32	-0.17	$4.2 \times 10^8$	$8.4 \times 10^8$			
80	II	0.19	-0.12	$8.0 \times 10^8$	$9.6 \times 10^8$	1.2	(3.0)	0.8
85		0.18	-0.12	$8.4 \times 10^8$	$1.0 \times 10^9$			
90		0.15	-0.10	$9.1 \times 10^8$	$1.1 \times 10^9$			
110	III	0.04	0	$1.2 \times 10^9$	$1.2 \times 10^9$	1.0	5.9	0.5
120		0.03	0	$1.4 \times 10^9$	$1.4 \times 10^9$			
130		0.03	0	$1.7 \times 10^9$	$1.7 \times 10^9$			
140		0.02	0	$2.1 \times 10^9$	$2.1 \times 10^9$			
(B) Hydrated to 7 wt %								
-20	I	0.33	-0.11	$2.7 \times 10^7$	$5.4 \times 10^7$	2	(3.0)	1.4
-10		0.33	-0.11	$3.8 \times 10^7$	$7.6 \times 10^7$			
0		0.33	-0.11	$4.7 \times 10^7$	$9.4 \times 10^7$			
10		0.33	-0.11	$5.6 \times 10^7$	$1.1 \times 10^8$			
30		0.33	-0.11	$9.0 \times 10^7$	$1.8 \times 10^8$			
40		0.32	-0.11	$1.3 \times 10^8$	$2.6 \times 10^8$	1.2	(4.1)	0.8
50		0.32	-0.11	$1.9 \times 10^8$	$3.8 \times 10^8$			
60		0.31	-0.11	$2.6 \times 10^8$	$5.2 \times 10^8$			
70	II	0.19	0	$8.5 \times 10^8$	$1.0 \times 10^9$	1.0	(7.1)	1.4
80		0.17	0	$1.0 \times 10^9$	$1.2 \times 10^9$			
90		0.14	0	$1.2 \times 10^9$	$1.4 \times 10^9$			
120	III	0.022	0	$2.0 \times 10^9$	$2.0 \times 10^9$	1.0		0.6

<sup>a</sup> Estimated errors:  $\pm 2\%$  in  $\langle D_{00}^2 \rangle$ ,  $\pm 30\%$  in  $\langle D_{02}^2 + D_{0-2}^2 \rangle$ ,  $\pm 10\%$  in  $R_{\perp}$ ,  $\pm 20\%$  in  $N$ ,  $\pm 0.1 \text{ G}$  in  $T_2^{*-1}$ . <sup>b</sup> See footnotes to Table IA.

TABLE III: Parameters for Molecular Ordering and Anisotropic Rotation for 5PC in DPPC Hydrated to 3 wt %<sup>a, b</sup>

$t, ^\circ\text{C}$	phase	$\langle D_{00}^2 \rangle$	$R_{\perp}, \text{s}^{-1}$	$R_{\parallel}, \text{s}^{-1}$	$N$	$T_2^{*-1}, \text{G}$
50	I	0.64	$6.0 \times 10^6$	$6.0 \times 10^7$	10	1.5
60		0.64	$1.2 \times 10^7$	$1.2 \times 10^8$		
70		0.64	$2.0 \times 10^7$	$2.0 \times 10^8$		
80	II	0.46	$1.2 \times 10^8$	$2.4 \times 10^8$	2	1.0
90		0.41	$1.6 \times 10^8$	$3.2 \times 10^8$		
110	III	0.21	$5.0 \times 10^8$	$5.0 \times 10^8$	1	1.0
130		0.16	$6.0 \times 10^8$	$6.0 \times 10^8$		

<sup>a</sup> Estimated errors: 4% in  $\langle D_{00}^2 \rangle$ ,  $\pm 20\%$  in  $R_{\perp}$ , and  $\pm 50\%$  in  $N$ . <sup>b</sup> See footnotes to Table IA.

limiting cases summarized elsewhere<sup>15b</sup> usually suffice in analyzing the spectra. In general, when  $N > 1$ , one may regard  $R_{\parallel}$  as the diffusion coefficient for either rotation about the  $z'$  symmetry axis or alternatively for internal rotational motion of the nitroxide moiety about an (composite) internal axis collinear with the  $z'$  axis. This is because  $R_{\parallel}$ , the diffusion coefficient for internal rotation, has a nearly equivalent effect on the spectrum as  $R_{\perp}$ . The choice whether to ascribe an  $R_{\parallel} > R_{\perp}$  to the effects of internal motion or to the overall motion must then be based on physical insight. For 16PC there is sufficient flexibility that both  $R_{\parallel}$  and  $R_{\perp}$  could be significantly determined by the modes of chain motions, while for 5PC they more likely contribute mainly to  $R_{\parallel}$ .

Spectra from several samples hydrated to higher water content (<15%) were also analyzed. Some of these results are shown in Figure 9, and some will be discussed in the next section. We show in Figure 13 some results we have obtained from a dispersion sample of 16PC in DPPC with 7% water. Included is the simulation based upon the data in Table IIB from oriented samples. This simulation was obtained by integrating simulations of oriented spectra for all tilt angles  $\theta$  equally weighted on the unit sphere. (In past simulations of dispersions we have found that the  $0^\circ$  and  $90^\circ$  angle components tend to dominate their features.<sup>15c</sup>) It shows good, but not perfect, agreement with experiment. In particular, the spectra for phase II correspond to the incipient slow-motional regime for which the details of the dispersion spectra are extremely sensitive to small changes in the parameters.<sup>15c</sup> (Also, the possibility of small differences between the microscopic properties of macroscopically oriented samples and of dispersions does exist; cf. ref 16.)

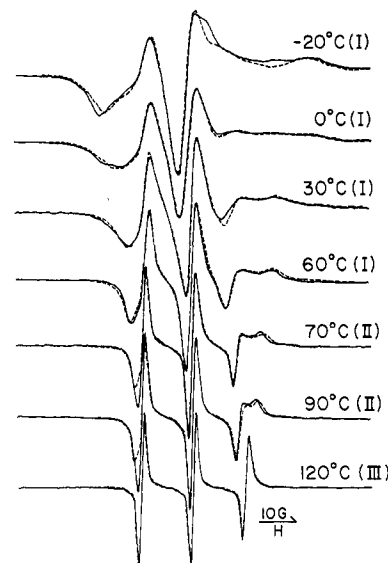


Figure 13. ESR spectra of 16PC in unoriented DPPC dispersions with 7 wt % water in a tube: (—), experimental spectra; (---), simulations based upon the parameters in Table IIB.

#### IV. Discussion

As is easily discerned from the structures of the nitroxides CSL, 5PC, and 16PC illustrated in Figure 1, these nitroxides are expected to report on the hydrocarbon chains of the lipid in different ways. The rigid and elongated nitroxide CSL, which is also hydrophobic, probes the average ordering of the chain skeleton (major part of chain) by aligning its long axis relative to the chains. It is thus a measure of the overall molecular alignment. The DPPC derivatives 5PC and 16PC report directly on the respective local portions (the vicinities of 5th and terminal carbons) of the chain, to which the nitroxide moiety is attached. This reflects not only the overall molecular alignment but also the local chain flexibility in the region of the spin-label. We interpret our results while taking these features of the respective nitroxides into account.

**Biaxial Gel Phase.** Recent NMR studies<sup>24,26</sup> of DPPC dispersions have presented some features differing from the previously held view<sup>6,7,36</sup> of an extended all-trans conformation with no

disordered segmental motion of the hydrocarbon chain in the crystalline phase. A deuterium NMR study<sup>24</sup> of perdeuterated DPPC dispersions does not support a model of the gel phase wherein the hydrocarbon chains are fully extended in a rigid all-trans form. This study also indicates that a large fraction of the lipid molecules cease their rotation about their long axes at a temperature near 0 °C. Corresponding to these results, saturation transfer ESR<sup>25</sup> shows a rapid decrease in the rate of rotational diffusion of the chain at temperatures below 20 °C. However, it is reported from a proton NMR study<sup>26</sup> of DPPC dispersions that at -15 °C there is still a significant amount of methylene chain motion or disorder. The present results listed in Tables I-III are consistent with the above results on the presence of chain motion and disorder but, in addition, reveal some detailed aspects relating to the following matters. (1) In the temperature range of ~40-70 °C in the gel phase, the chain motions of 5PC and 16PC are still significant (with rates of  $10^6$ - $10^8$  s<sup>-1</sup>). However, anisotropy in the rotational diffusion is highest in this phase. (2) The rates of diffusional motion of the hydrocarbon chain differ by an order of magnitude between the central (5th) portion and terminal portion as represented by values of  $\bar{R} = 2.4 \times 10^8$  and  $2.4 \times 10^7$  s<sup>-1</sup> at 50 °C for 16PC and 5PC, respectively. The high value of  $\bar{R}$  for 16PC indicates fast segmental motion around the terminal C-C bond. (3) The ordering of all the spin probes remains constant throughout the gel phase, in contrast to the motions which are thermally activated processes (Figures 10 and 11). This could be explained in terms of modes of motion in the gel phase which remain unchanged. (4) The chain disorder and/or distortions in the local positions (5th and terminal position), probably related to segmental chain motions, can be inferred from  $S$  values that are lower in 5PC and 12PC than in CSL ( $\langle D_{00}^2 \rangle$  ( $\equiv S$ ) = 0.90 in CSL, 0.64 in 5PC, and 0.32 in 16PC). The disorder is largest at the terminal portion as further evidenced by the significant asymmetry term in the ordering for 16PC.<sup>37</sup> However, the lipid as a whole is still (in the time average of the chain motions) close to an extended structure, as inferred from the very high  $S$  and  $N$  values of CSL,  $N (= R_{\parallel}/R_{\perp}) = 150$ .

Figure 12 shows the Arrhenius plot of  $\bar{R}$  for 16PC in DPPC hydrated to 7%, ranging from 60° (just below  $T_c$ ) to a lower temperature (-20 °C). It is seen in this figure that the slope changes at ca. 20 °C, suggesting a change in the mode of chain diffusion at this temperature. The activation energy was determined to be  $7.1 \pm 1.5$  kcal/mol in the upper temperature range (30-60 °C) and  $3.0 \pm 0.6$  kcal/mol in the lower range (-20 to +10 °C), keeping  $N = 2$  over the whole range. On the other hand, in this lower temperature range, the spectra for 5PC are almost unchanged, implying motions too slow to be detected. In previous <sup>2</sup>H NMR<sup>24</sup> and STESR<sup>25</sup> studies it was concluded that hydrocarbon chain motion ceases at 0-20 °C. Our results on 5PC are consistent with this provided we regard the motions as too slow to be detected rather than "frozen out". However, our results with 16PC show that the terminal methyl group still exhibits motion even at -20 °C. The reduced activation energy might imply that rotations about the terminal C-C bond can occur more easily once the major parts of the chains become more rigid. (By the major part of the chain, we mean approximately the first ten methylene groups of the palmitoyl chains<sup>38a</sup>.) A significant amount of methylene motion at -15 °C observed by <sup>1</sup>H NMR<sup>26</sup> may thus reflect the rotation of the terminal methyl group.

(36) Cameron, D. G.; Casal, H. L.; Mantsch, H. H.; Boulanger, Y.; Smith, I. C. P. *Biophys. J.* **1981**, *35*, 1.

(37) This flexibility gradient is, of course, well-known (cf.: Berliner, L. J., Ed. "Spin-Labeling—Theory and Applications"; Academic Press: New York, 1976; Chapters 12 and 13). We are able to quantify the flexibility gradient in terms of the reduced ordering and its symmetry, as well as the increased motional rate and its reduced asymmetry (cf. also ref 15c).

(38) (a) Seelig, A.; Seelig, J. *Biochemistry* **1974**, *13*, 4839. (b) These authors criticize the determination of ordering by ESR methods, presumably because of the perturbing effect of the nitroxide, which could lower the ordering. The correspondence noted above between NMR results and our rigorous ESR analysis of well-oriented samples suggests that perhaps at least part of the previously published discrepancies may be due to imprecise methods used to interpret the ESR spectra.

*The New Phase Transition in the Liquid-Crystalline Phase.* As already noted, we have found a phase transition occurring at 100-110 °C. In order to characterize this transition (second transition), we compare the change in the ordering  $S$  and diffusion constant  $\bar{R}$ , at temperatures just below and above the two-phase region for this second transition, vs. the corresponding change induced by the first or main transition. From the data at 70 and 80 °C and also 90 and 110 °C in Tables I-III, it is found that the ordering parameter  $S$  experiences a more significant relative reduction at the second transition compared to that at the main transition (i.e. by factors of 0.42, 0.51, and 0.27 for CSL, 5PC, and 16PC, respectively, at the second transition and by 0.84, 0.72, and 0.59, respectively, at the main transition). On the other hand, the diffusion coefficient  $R_{\perp}$  for the chain probes (i.e. 5PC and 16PC) experiences a more significant relative increase (i.e. by factors of 6 and 2.7 for 5PC and 16PC, respectively, at the main transition and by 3.2 and 1.3, respectively, at the second transition). We thus regard the second transition as an "orientational type" leading to a significant "melting" of the orientational order of the lipid hydrocarbon chains but a smaller increase in fluidity, as measured by  $R_{\perp}$  in comparison to the main transition. The main transition, on the other hand, shows only a moderate decrease in ordering but a more substantial increase in  $R_{\perp}$  for the chain probes. Thus, a relatively smaller reduction in molecular ordering more effectively "unfreezes" the chain motions at the main transition. The relative increase in  $R_{\perp}$  for CSL at the two transitions is, however, comparable (i.e. by factors of 8.2 and 11 at the main and second transitions, respectively), suggesting that while local chain motion increases more significantly at the main transition, the overall molecular motions exhibit comparable relative changes at both phase transitions. Also, while  $R_{\perp}$  shows substantial change at the phase transitions,  $R_{\parallel} = NR_{\perp}$ , which measures the motion about the long chain axis, is much less affected by the phase transitions. This undoubtedly reflects the existence of significant motion of this type in the gel phase, which may be due to its relatively unhindered nature. In fact,  $R_{\parallel}$  values for CSL and 5PC are comparable (with that for 16PC only about 3 times faster) in phases I and II even though their  $R_{\perp}$ 's are at least an order of magnitude different (i.e. the respective  $R_{\perp}$ 's obey CSL  $\ll$  5PC  $\ll$  16PC) in these phases.<sup>39</sup>

We can also comment on the relative differences of the phase transitions with respect to position along the chain. At both phase transitions there is a more significant relative reduction in ordering at the end of the chain but a smaller increase in fluidity (as measured by  $R_{\perp}$ ). Thus, while there is greater "melting" of orientational order at the end of the chain, the end-chain motions are not as significantly tied to the ordering.

Lastly, we comment on the liquid-crystalline phase III vs. the isotropic phase (phase IV). We have not extensively studied this transition, except for results with CSL shown in Table I. At this transition, the residual ordering is, of course, lost, but there is hardly any change in motional rates. Thus, liquid-crystalline phase III appears already to be very fluid with its fluidity largely unaffected by the small amount of ordering in this phase, except perhaps for an estimated value of  $N$  somewhat larger than the value  $N = 5$ , characteristic of CSL in isotropic fluids (and found for the isotropic phase, phase IV). These trends bear a striking similarity to observations typical of isotropic-nematic phase transitions in thermotropic liquid crystals, and one wonders whether there might be some validity to a comparison of liquid-crystalline phase III to a thermotropic nematic while phase II is to be compared to a thermotropic smectic. While nematics show

(39) In assigning how changes in ordering affect the rates of molecular motions, we note that, in the high ordering limit, the effective diffusional rate  $R_{\perp}$  in the mean cylindrical restoring potential of the surrounding molecules becomes  $\lambda R_{\perp}$  for our model (cf. ref 11b). As the temperature is increased through the phase transitions,  $\lambda$  decreases while  $R_{\perp}$  increases. Thus, the net change on the perpendicular diffusion rate at the phase transition is somewhat less dramatic. We also note that substantial variations in  $N$  for the different phases could have a possible alternative explanation in terms of fluctuating torque or other more sophisticated mechanisms (cf. ref 12, 15, and also: Meirovitch, E.; Freed, J. H. *J. Phys. Chem.* **1980**, *84*, 2459; **1984**, *88*, 4995).

a substantial temperature-dependent variation in ordering similar to that in phase III, the ordering in phase III (as evidenced by CSL) appears to be significantly smaller than typically found for nematics. Also, the second transition, in showing a very substantial change in  $S$ , is unlike a nematic-smectic transition, wherein  $S$  hardly changes. Furthermore, we have no evidence to suggest that the multibilayer (or smectic) ordering is lost.<sup>40</sup>

Our observations on the second transition in DMPC are similar to those for DPPC. For example, the second transition starts to occur when  $S = 0.67$  for CSL in DPPC and when  $S = 0.60$  for CSL in DMPC. (For CSL in DMPC hydrated to 3%,  $S = 0.86$  in the crystalline phase; it ranges from 0.75 to 0.60 over the temperature range 60–95 °C and is <0.20 above 120 °C.)

We would now like to point out interesting similarities between our observations and recent theoretical predictions of Kimura and Nakano<sup>23</sup> based on their simplified model for orientational phase transitions in systems of flexible molecules. They present a simplified, hence more convenient, model than that used by Marcelja.<sup>41</sup> They use a molecular field approximation involving two order parameters:  $S$ , the orientational order parameter, and  $\sigma$ , the parameter reflecting the mean conformation of the chains. They describe the main transition as involving a cooperative change in the conformation of the hydrocarbon chains of the lipid molecules from "an extended long form to a bent short one" (i.e.  $\sigma$  decreases) with a simultaneous decrease in orientational order. What is most interesting to our work is their prediction of a second transition under certain circumstances roughly associated with having flexible chains. They predict such a second transition for DMPC and DPPC and relate it to the secondary phase transition observed by Mitsui and Furuya.<sup>2</sup> This is a calorimetrically weak transition<sup>2,3</sup> occurring at 62 °C in the liquid-crystalline phase of DPPC bilayers and monolayers under conditions of excess water. In their model there is a large drop in  $S$  (going to zero) but only a small change in  $\sigma$ , the conformation parameter, at the second transition. We do observe a small residual ordering ( $S \neq 0$ ) at the second transition, but Kimura and Nakano may have oversimplified their model in ignoring effects of polar head groups and of repulsive forces. Their prediction of only a small change in  $\sigma$  might be correlated with the rather small changes in motional rate we observed for the chain probes at the second transition. Their model, however, does not clarify any difference between the second transition and the transition to an isotropic phase. They are thus led to a different correlation between lipid-phase transitions and those of thermotropic liquid crystals from what we have suggested above.<sup>42</sup>

**Dependence of Ordering and Diffusion on Water Content.** We have mainly discussed our results on the DPPC samples hydrated to 3%. Here, we comment on our results analyzed for samples hydrated to higher water content ( $\leq 15\%$ ). In the gel phase, constancy of ordering,  $S$ , vs. temperature was also found for 7% water ( $S = 0.88$  for CSL, 0.64 for 5PC, and 0.32 for 16PC; cf. Tables IB and IIB). The value of  $S$  was moderately reduced with an increase of the water content, as represented by the values for CSL (0.90 to 0.78 on going from 3% to 15%). The  $\bar{R}$ 's for 7% water ( $3.7 \times 10^6 \text{ s}^{-1}$ ) for CSL and  $1.8 \times 10^8 \text{ s}^{-1}$  for 16PC at 40 °C) were slightly higher than those for 3% as shown in Tables I and II. Such small effects of water content on the chain ordering and diffusion in the crystalline phase can be understood in terms of just the small increase<sup>22</sup> of the surface area per lipid molecule in its hexagonal packing. In the liquid-crystalline phase, the  $S$

(40) In fact, the annealing methods utilized to improve sample alignment require that the sample be just below the isotropic phase in phase III. Samples so prepared will remain defect free when cycled through phases I–III. We believe this implies that all these three phases preserve the multibilayer lamellar (or smectic A) alignment.

(41) Marcelja, S. *J. Chem. Phys.* 1974, 60, 3599.

(42) Added in Proof: It appears to us that it might be important to consider the polar head-group region. The fact that this is a reversible transition and it appears near 100 °C in both DPPC and DMPC suggests to us that it might be driven by thermally activated motion of the water molecules which hydrate the polar head groups. This could weaken the interaction between the polar head groups enabling the transition to much weaker ordering without a very large change in motion of the hydrocarbon chains.

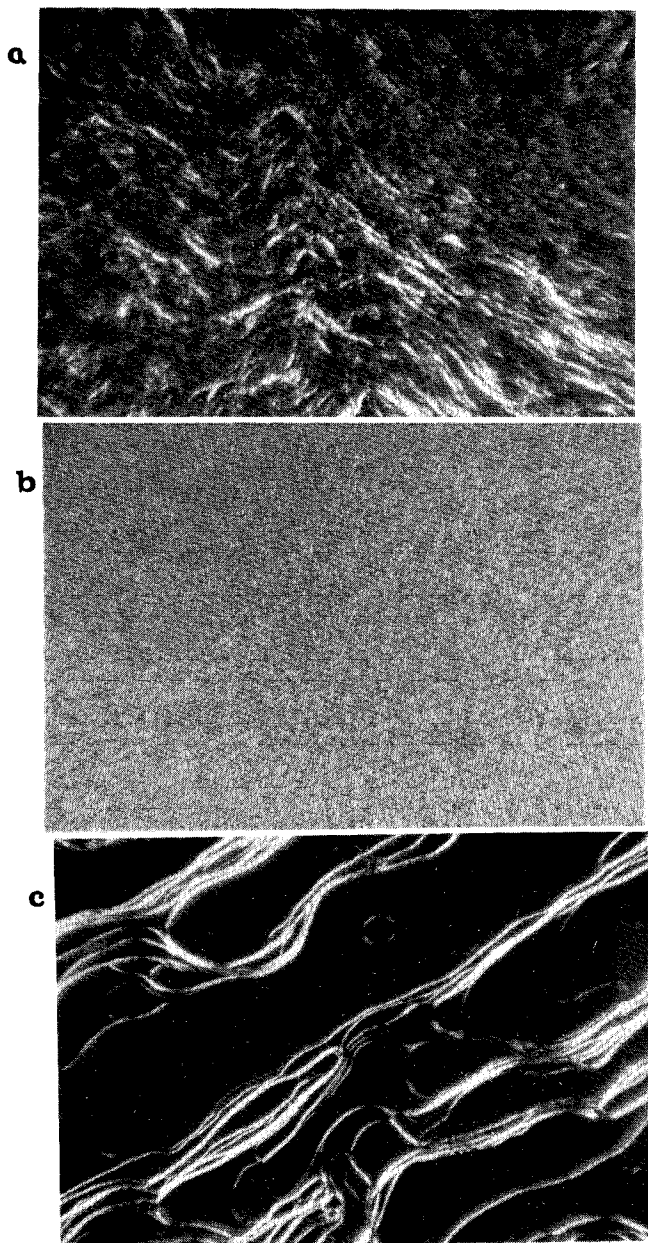


**Figure 14.** Defects observed between crossed polarizers: (a) unoriented starting materials at room temperature, (b) polygonal arrays at 80 °C, (c) oily streaks at 60 °C.

and  $\bar{R}$  values are strongly dependent on water concentration, as shown by the data for CSL in DPPC at 70 °C in Figure 9. However, when compared at the same  $\Delta T \equiv T - T_c$ , they were found to closely approach each other. For example, the  $S$  values of CSL in DPPC converge to 0.73–0.76 at  $\Delta T = +10$  °C in the range of 2%–20% water investigated. This indicates that the change in molecular ordering brought about by the main transition is almost independent of the water content. The  $S$  values of 5PC and 16PC at 80 °C, i.e. just above  $T_c$ , are 0.46 and 0.19, respectively. These agree well with 0.46 and 0.21 at 41 °C just above  $T_c$  for the 5C and 15C selectively deuterated DPPC's, respectively, determined by <sup>2</sup>H NMR<sup>38a,b</sup> on dispersions with excess water. This correspondence may confirm our view that at  $T_c$  the equilibrium properties of the lipid chains are essentially independent of water content.

## V. Summary and Concluding Remarks

The purpose of this study, viz. the assignment and characterization of the phases and phase transitions of DPPC and DMPC in the low water content region ( $\leq 15\%$ ) from the viewpoint of the hydrocarbon chain orientation and diffusion as probed with

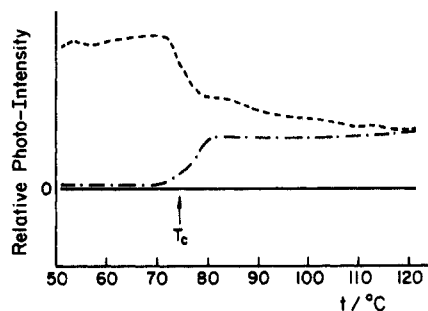


**Figure 15.** Transmitted photointensities vs. temperature for (—) defect-free samples and samples with (---) defect (a) and (---) defect (b).

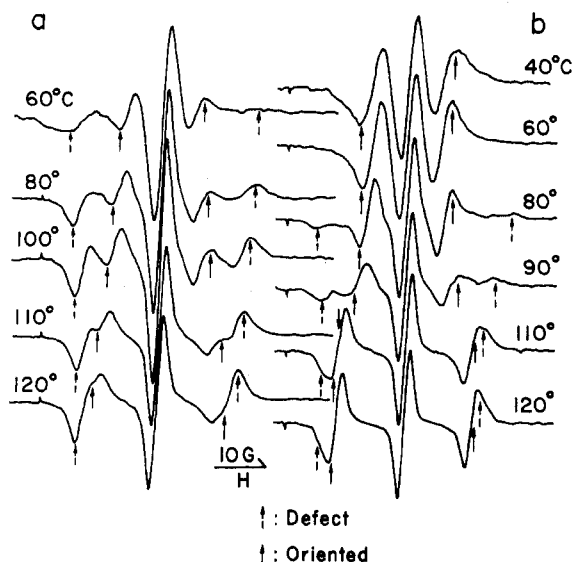


**Figure 16.** ESR spectra of CSL in oriented samples at 3% water ( $t_{I-II} = 75$  °C) with defects for  $\theta = 0^\circ$ : (a) unoriented starting materials (area 65% at room temperature); (b) polygonal-array defects (area 37% at 80 °C).

nitroxide spin-labels, was satisfactorily accomplished by the use of oriented ESR samples and careful spectral simulation. The new "chain-orientational" transition found in the liquid-crystalline phase was compared to a recent statistical theory on the chain configuration and lipid-phase transitions. In comparison with this second transition, the main transition could be regarded as primarily a "chain-diffusional" transition. From this study, the following scheme was established for the respective phase transitions: biaxial gel phase I—liquid-crystalline Phase II—liquid-crystalline phase III—isotropic phase IV. In the phase I, the major portion of the hydrocarbon chain has high orientational order, suggesting an extended structure in its equilibrium state, although local portions in the chain exhibit some disorders. The rotational diffusion rates about axes perpendicular to the main chain axis differ by an order of magnitude between the major portion (i.e. 5th carbon) and terminal portion of the hydrocarbon chain. On decreasing the temperature in the phase, the diffusion of the major portion of the chain is substantially slowed down near 20 °C while that of the terminal portion continues to occur even in the lower temperature range (−20 to +10 °C). With respect to the liquid-crystalline phase, we emphasize that in phase II the overall chain order is still close to that of the crystalline phase, in contrast to past work wherein it has usually been assumed that there is (almost) no long-range ordering of the chains in the liquid-crystalline phase. The main feature with which to characterize phase II in comparison with the crystalline phase I is the large increase in rotational diffusion (i.e. in  $R_{\perp}$ ) but only moderate decrease in ordering. There is, however, a substantial decrease in the orientational order in passing into liquid-crystalline phase III with a less significant increase in motional rate.

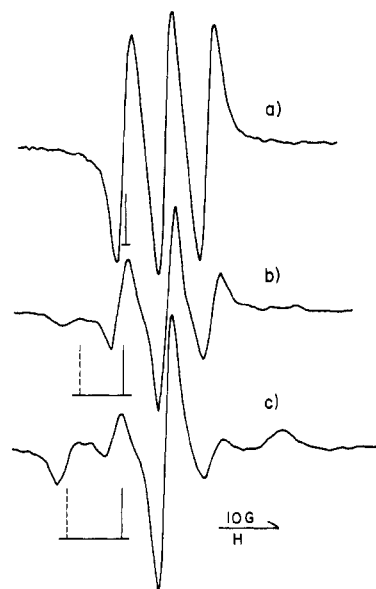


**Figure 17.** ESR spectra of CSL for  $t = 80$  °C and  $\theta = 0^\circ$  in phase II: (a) aligned sample without defects, (b) aligned sample with polygonal-array defects, (c) aligned sample with unoriented starting materials. Vertical solid lines mark spectra from aligned areas, while vertical dashed lines note those from defect areas, and the vertical broken line denotes the *apparent* center of the  $M = 1$  line.

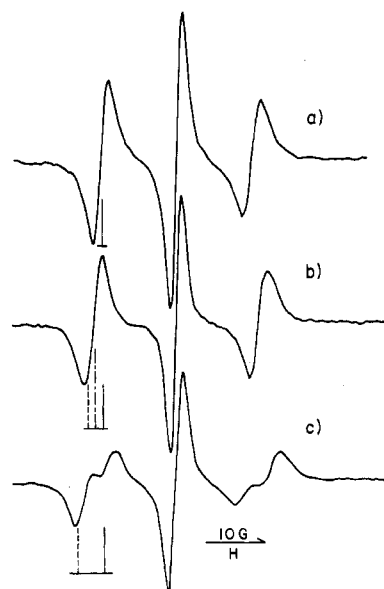


**Figure 18.** ESR spectra of CSL in 3 wt % H<sub>2</sub>O-DPPC samples with and without defects for  $t = 110$  °C and  $\theta = 0^\circ$  in phase III. Other details as in Figure 17.

The above remarks apply over the low water content region ( $\leq 15\%$ ) which we investigated in this work. A more detailed picture of the chain order and diffusion may be obtained by further studies including the use of additional selectively nitroxide-labeled DPPC's. Also, in this work, we have not dealt with any (presumably small) variations in the local director from the mean macroscopic director, although some deviations between predicted and observed spectra in the crystalline phase (cf. Figure 8) might be due to such effects. The behavior of the polar head groups of lipids within the phases and at the phase transitions is a very interesting subject which may be investigated by the use of head-group spin probes.<sup>42</sup>

We have demonstrated, throughout this study, the great value of utilizing oriented lipid samples of well-defined quality in magnetic resonance studies combined with accurate spectral simulations.

**Acknowledgment.** We thank Professor G. W. Feigenson of Cornell University for gifts of 5PC and 16PC, Dr. Leela Kar for many helpful discussions, and Dr. Yuhei Shimoyama for a critical reading of the manuscript. This work was supported by NIH Grant GM 25862.

#### Appendix: Analysis of Defects and Their Effects on ESR Spectra

Some additional results related to this paper are presented in this section.

1. *Types of Defects Observed.* The following types of defects were observed under crossed polarizers with our samples.

(a) *Unoriented Starting Materials.* This type with no regular and repeated texture was assigned to the starting polycrystalline materials left unoriented after the alignment procedure (thus it does not belong to the category of defects in a true sense). This type occurs through insufficient compression with the compression technique and also through rapid change of temperature and water content. The large domains are often observed on boundaries between air (or steam) bubbles and the surrounding oriented areas when Powers<sup>22</sup> annealing technique is applied to our ESR sample preparation. The other types of defects are ultimately changed to this type in their time evolution. A photograph of this defect is shown in Figure 14a.

(b) *Polygonal-Array Defects.* On raising the temperature, these defects first appear at  $T_c$ , and then the individual polygons grow in size and often change in type (a) in the upper temperature range ( $>100^\circ\text{C}$ ) of the liquid-crystalline phase ( $L_\alpha$  phase) (cf. Figure 14b). With our ESR samples, this type often appears in a few days after alignment. It is also produced by detaching the glass plate of the sample sandwich from the oriented lipid layer on a part of the sample area, indicating sample dilation as a major origin for its appearance.

(c) *Oily Streak Defects.* This type appears through insufficient compression and also rapid cooling after the alignment procedure (cf. Figure 14c).

(d) *Strandlike Defects.* This type is sometimes produced in an oriented region by the rapid change of temperature. These appear as just a few lines under the microscope.

(e) *Fine Dot Defects.* Only this type is not listed in Asher's paper.<sup>21</sup> We have found this type a few times when the water content of the multilayers has been increased by use of a humidity technique or by a submersion technique. This type is similar morphologically with the polygonal-array type (b) but can exist also in the crystalline phase. It appears as fine white dots on an otherwise black background.

2. *Major Defects and Alignment Techniques.* Major defects occurring in our ESR samples are types (a) and (b) from the view of both frequency and extensiveness. These defects seem to occur more frequently and extensively in our ESR samples than in the optical samples (Asher's samples<sup>20</sup> and Powers' samples<sup>22</sup>), even if the alignment principles are the same for the ESR and optical samples. This comes from the difference in the geometry and form of the sample used: they (Asher,<sup>20</sup> mechanical alignment technique, and Powers,<sup>22</sup> annealing technique) used a big sample assembly consisting of slide glasses, spacer, and mechanical press. The use of the assembly enables them to keep uniform thickness and proper pressure over an entire sample region and hence to suppress the occurrence of defects. We used thin glass plates (cover glass), no spacer, and an adhesive instead of their corresponding substances. Therefore, in our sandwich form, the defects occur easily due to nonuniform thickness, distortion (or strain) of glass plates, and/or dilation of the sample sandwich. With the compression technique used in this study, the difficulty was conquered by preparation of thin-layer samples (10  $\mu\text{m}$  in typical thickness). If the sample conditions similar to those for the original samples could be realized for ESR sample preparation, it should be possible to prepare thicker defect-free monodomains of oriented ESR samples. Significantly thicker samples have been produced in our laboratory but with small amounts ( $<10\%$ ) of defects.<sup>43</sup>

3. *Factors Leading to the Instability of Macroscopic Orientation.* The following factors make oriented samples unstable through reduction of ordering interactions.

(a) *Increase of Temperature.* In general, the macroscopic orientation of lipid samples is less stable above  $T_c$ . The multilayer form sandwiched between glass plates is better than the film form produced by an evaporation technique in temperature stability.

(b) *Increase of the Water Content.*

(c) *Introduction of Polypeptide (Gramicidin A).* Therefore, to prepare defect-free samples containing water at higher contents and/or GA, one requires a skillful technique during the alignment procedure.

4. *Factors Leading to Reduced Reproducibility of ESR Spectra of Oriented Samples.* (a) *The Presence of Defects.* This can be detected optically with a polarizing microscope (i.e. morphology and transmitted photointensity).

(b) *Change of the Water Content.* The sample preparation and measurement at higher temperatures ( $\geq 100^\circ\text{C}$ ) cause a reduction of the water content. The water content should be calibrated by a proper method. In the low water content region ( $\leq 15\%$ ), the main transition temperature can be used as a measure of the water content involved between bilayers, because the temperature is sensitive to the water content.

(c) *Chemical Quality of Lipid.* We have observed two-component ESR patterns a few times when we used, for sample preparation, commercial lipids that have stood for a long time after being unsealed. In this case, the whole sample area appeared black under crossed polarizers. It was inferred that the oriented samples consisted of two regions of which one was rich in the decomposed products of lipid and the other was deficient in them. The areas rich in the decomposed products may form an isotropic phase which also appears black under crossed polarizers. Therefore, lipids should be checked for chemical quality before use and also should not be kept, for a long time, at higher temperatures ( $\geq 100^\circ\text{C}$ ) in the process of sample alignment.

5. *Limitations of ESR Measurements at Higher Temperatures ( $>100^\circ\text{C}$ ).* The following factors imposed restrictions on the ESR measurements of higher water content ( $>10\%$ ) samples at higher temperatures ( $>100^\circ\text{C}$ ).

(a) *Escape of the Water from the Bilayers.* When performing ESR measurements above  $100^\circ\text{C}$ , the water concentration is reduced usually to below 8%. This problem may not be improved by use of an Asher- or Powers-type sample assembly (cf. ref 20 and 22).

(b) *Chemical Decomposition of Nitroxide.* The ESR signals of nitroxides (CSL and 16PC) were rapidly reduced through the higher temperature measurements of higher water content samples. This may be caused by hydrolysis of the N-O bond at higher temperatures. A similar problem was brought about by the presence of GA.

6. *Correspondence between Polarizing Microscopy and ESR. Results with respect to Defects Involved in Oriented Samples.* We investigated the correspondence between polarizing microscopy (PM) and ESR, using the samples containing the "most popular defects", i.e. unoriented starting materials (a) and polygonal-array defects (b). Figure 15 shows transmitted photointensities vs. temperature for our thin-layer samples (20–30  $\mu\text{m}$ ). A jump in the intensity at  $T_c$  observed for defect (b) corresponds to first occurrence of the defect. The rapid decrease at  $T_c$  observed for defect (a) does not mean a decrease in the quantity of the defect. This can be explained in terms of a change in the optical birefringence at  $T_c$ . The quantity of defect (a) of the sample used for this measurement was not changed over the whole temperature range ( $\leq 120^\circ\text{C}$ ). Figure 16 shows the ESR spectra of the corresponding samples. We see two-component patterns in the whole temperature range ( $\leq 120^\circ\text{C}$ ) for the sample with defect (a) and one pattern only in the liquid-crystalline phase (80–120  $^\circ\text{C}$ ) for the sample with defect (b). Thus, PM and ESR results correspond qualitatively to each other. The outer and inner components in the ESR spectra can be assigned respectively to the defects and oriented areas. This was confirmed semiquantitatively by measurements of the transmitted photointensity. In

(43) Kar, L.; Ney-Igner, E.; Freed, J. H. *Biophys. J.*, submitted for publication.

thin samples, defects, irrespective of the type, appear white (bright) under crossed polarizers. This phenomenon could be used to estimate the area occupied by defects in the entire sample region, through averaging the photointensities measured at local areas. The defect-free sample and nearly "100%-defect" (i.e. unoriented starting material) sample were used as standards. The results showed that the outer component is reduced in ESR signal intensity with decrease in the defect area determined optically. A simple relation was found for pure lipid samples (CSL and 16PC); viz. defect-free samples yield a simple triplet and defect-containing samples yield a two-component type of spectrum.

The observation of defect signals depends on the line width and ordering and so on the water content, temperature, and nitroxide. The defect signals were best observed in the liquid-crystalline phase II (80-90 °C at 3% water) of CSL samples. In the case of 16PC, the defect signals from samples containing as much as 50% of their

area as defects were not resolved near room temperature. Therefore, a polarizing microscope is in general better for defect detection than ESR. The ESR spectra of defect-free samples exhibited good reproducibility when the conditions of water content, lipid quality, etc. were well-defined.

Figures 17 and 18 show a comparison of the ESR signals from defects (a) and (b) in the liquid-crystalline phases II and III. The respective types of defects produced slightly different signals in their apparent splitting and broadening, which reflect on the macroscopic structure intrinsic to the respective defect (cf. ref 20). However, to a rough approximation, the angular ( $\theta$ ) dependence of the apparent splitting in the spectrum from the defects appears to be negligible.

Registry No. DPPC, 2644-64-6; DMPC, 13699-48-4; cholestan-3-one, 15600-08-5.

## Analysis of a Phase Transition at 134 K in Decanoic Acid by Infrared Spectroscopy

D. B. West and H. L. Strauss\*

Department of Chemistry, University of California, Berkeley, California 94720 (Received: June 22, 1984)

Using infrared spectroscopy, we have discovered a small phase transition at 134 K in pure decanoic acid ( $n\text{-C}_{10}\text{H}_{20}\text{O}_2$ ). Differential scanning calorimetry shows it to be a sharp, first-order transition with  $\Delta H \sim 15$  cal/mol. Examining the effects of the transition on the vibrational modes of the hydrocarbon chain, we can determine the slight change in the crystal structure resulting. Two other possible phase transitions occurring below 100 K are discussed, one of them related to the bizarre infrared spectral changes occurring at low temperatures which were explained by Umemura and Hayashi. The phase behavior discovered here has a strong dependence on the water content of the decanoic acid, and it may be possible to relate it to the more complicated phase behavior of lipid systems and biological membranes.

### Introduction

In recent years it has become apparent that the solid-to-liquid-crystal phase transition discovered in model lipid systems is important in biological membranes.<sup>1</sup> In the same way, the elucidation of solid-solid phase transitions in fatty acids may be useful in suggesting what sort of temperature-dependent structural changes are possible in membranes or other lipid-containing systems. Specifically, the crystal structure of decanoic acid, with its planes of carboxylic head groups and hydrocarbon tails extending out from these planes, looks very much like the lipid bilayers in membranes and so may serve as a model for them. In this paper we report the discovery of a small phase transition (and two other probable phase transitions) in decanoic acid and analyze the associated structural change in detail using infrared spectroscopy. In addition to allowing understanding of the structural changes described in this paper, our interpretation of the infrared measurements on decanoic acid may aid the interpretation of vibrational measurements on complicated biological systems containing fatty acids or fatty-acid-like components.<sup>2</sup>

Long-chain fatty acids form dimers in the solid state, the two head groups making an eight-membered ring with two hydrogen bonds. The crystal structure studied here is the C form of the polymorphic normal fatty acids which is metastable (obtained from the melt irreversibly) for the acids having even numbers of carbons from 8 to 22.<sup>3</sup> This structure, shown in Figure 1, has the axis of the head group perpendicular to the  $ab$  plane of the monoclinic ( $P_{21}/a$ ) unit cell. The hydrocarbon chain is essentially parallel to the  $c$  axis, which forms an angle of 59° with the  $a$  axis.<sup>4</sup>

Umemura and co-workers have explained an anomaly in the infrared spectrum associated with the strong hydrogen bonding between the head groups of the normal fatty acids (described

below). In the process they performed a normal-coordinate analysis on decanoic acid which aided assignment of the spectrum.<sup>5</sup> The spectrum is comparable to that of an  $n$ -alkane but modified by the highly polar head group.

The vibrational spectrum of the hydrocarbon chain consists of progressions of bands arising from superpositions of the vibrational modes of the individual methylene groups. The frequency of each band in a progression is determined by the phase relationship between the vibrations of contiguous methylene groups. The phase relationships of the different modes in a progression of the eight-carbon chain of decanoic acid are depicted in Figure 2.

The hydrocarbon chain modes with transition moments perpendicular to the axis of the chain, such as the methylene stretching, bending, and rocking modes (Figure 2), have intensities comparable to the corresponding  $n$ -alkane modes.<sup>6</sup> The modes with transition moments along the chain axis, however, gain intensity from coupling with the strongly absorbing modes of the head group such as the hydroxyl and carbonyl oxygen stretches near 970 and 1700  $\text{cm}^{-1}$ , respectively.<sup>5</sup> Thus, the bands of the wagging, twisting, and carbon-carbon stretching progressions in normal fatty acids are 50-500 times more intense than the corresponding bands of the alkanes.

We use these well-assigned chain progressions to analyze, in a qualitative way, the changes in the molecular structure at the phase transition. Further, by a detailed analysis of the different bands of a particular progression, local information can be obtained. That is, we can determine whether changes in the conformation occur in the chain near the head group, in the middle of the chain, or at the methyl group.

### Experimental Section

The decanoic acid used was Aldrich Gold Label 99+% which we further purified by zone refining. Subsequent GC and TLC<sup>7</sup>

(1) Nagle, J. F. *Annu. Rev. Phys. Chem.* **1980**, *31*, 157.

(2) Luzzati, V.; Tardieu, A. *Annu. Rev. Phys. Chem.* **1974**, *25*, 79.

(3) Von Sydow, E. *Ark. Kemi* **1955**, *9*, 231.

(4) Malta, V.; Celotti, G.; Zannetti, R.; Martelli, A. F. *J. Chem. Soc. London, Ser. B* **1971**, 548.

(5) Umemura, J. J. *Chem. Phys.* **1978**, *68*, 42.

(6) Schachtschneider, J. H.; Snyder, R. G. *Spectrochim. Acta* **1963**, *19*, 85.